2011 11th IEEE-RAS International Conference on Humanoid Robots
Bled, Slovenia, October 26-28, 2011

Posture and Balance Control for Biped Robots based on Contact Force Optimization

Christian Ott, Maximo A. Roa, and Gerd Hirzinger

Abstract— **This paper presents a new balancing control approach for regulating the center of mass position and trunk orientation of a bipedal robot in a compliant way. The controller computes a desired wrench (force and torque) required to recover the posture when an unknown external perturbation has changed the posture of the robot. This wrench is later distributed as forces at predefined contact points via a constrained optimization, which aims at achieving the desired wrench while minimizing the Euclidean norm of the contact forces. The formulation of the force distribution as an optimization problem is adopted from the grasping literature and allows to consider restrictions coming from the friction between the contact points and the ground.**

I. Introduction

A good performance for a walking robot can be simply defined as moving from a starting to a goal point without falling down. In this sense, the main objective of the control in a walking robot is to guarantee a suitable ground reaction force to keep the dynamic balance. However, it is also desirable to have a controller that allows the robot to adapt (compliantly) to unknown external perturbation forces. Traditionally, a general strategy is to use a dynamics based walking pattern generation which provides the desired trajectories for underlying position controllers. However, due to the finite foot support area, pure position control is insufficient for executing these trajectories. Therefore, force sensors in the feet are usually integrated for implementing an inner force- or ZMP (Zero Moment Point) control loop. In that way, the desired contact state between the robot and the ground is ensured and control problems related to underactuation and their accompanying state estimation problems are avoided. While this approach allows the generation of a large range of stepping and walking motions for complete humanoid robots, it is limited to a restricted set of contact states. A position-based compliance control that allows the robot to adapt to external disturbances requires force measurement at every expected contact point, which increases the computational load and creates unavoidable time delays in the controller [1]. Other position-based balance compensators have been developed, although they share the same issues previously described [2], [3].

As an alternative to joint position controllers, recently several groups gained interest in the use of joint torque sensing and control for biped robots. The humanoid robot CB [4], built by Sarcos, uses hydraulic actuation and allows joint torque sensing. An impedance control for biped walkers, named Virtual Model Control, was proposed and used in robots in which torque control is enabled via series elastic actuation [5]. The DLR has developed a biped walking robot based on the torque controlled joint units of the DLR-KUKA Light-Weight Robot (Fig. 1), which can be position or torque controlled [6].

Fig. 1. DLR-Biped: A biped walking machine with torque controlled joints.

Passivity-based impedance and compliance controllers based on joint torque sensing were applied to manipulation tasks in [7], [8], wherein the joint torque feedback was motivated by a robot model with joint elasticities. In the context of biped balancing control, joint torque sensing and control was first used in [9]. Such controller provides gravity compensation and adaptation to unknown external forces. The method sets a desired applied force from the robot to the environment, then distributes that force among predefined contact points, and transforms it to the joint torques directly. The approach does not require contact force measurement or inverse kinematics or dynamics. The method can be extended to compensate for yaw perturbations, and to provide adaptability to unknown rough terrain [10]. The controller has been tested in simulation and on the CB robot [4].

More recently, a balancing controller based on the compensation of linear and angular momenta was proposed [11]. The approach controls independently the desired ground reaction force and center of pressure at each support foot, which allows it to deal with different ground geometry. The performance of the robot is shown with simulated experiments. In [12], contact force optimization was used for balancing based on the center of mass dynamics and was combined with virtual task forces. For the mapping of the contact forces to the joint torques, the nonlinear multibody dynamics was considered. In addition to the force

All the authors are with the Institute of Robotics and Mechatronics, German Aerospace Center (DLR), Wessling, Germany. E-mail: christian.ott@dlr.de

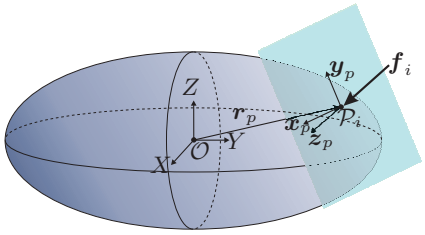

Fig. 2. Object and contact coordinate frames.

distribution, the handling of internal forces in multi-contact interaction tasks was studied in [13] based on the concept of a virtual-linkage model.

This paper proposes a new balancing controller to withstand external perturbations by distributing the required forces among predefined contact points. The approach reuses a formulation coming from the field of robot grasping to create a controller that keeps both the position and orientation of the robot. The force required to counteract external perturbations is distributed to the contact points via a constrained optimization problem.

The required background on frictional grasps is provided in Section II, and Section III discusses the dynamic model for the biped robot. Section IV describes in detail the design of the balancing controller. Section V presents the experiments showing the performance of the designed controller, both in simulation and on a real robot. Finally, Section VI summarizes the work.

II. Background on Frictional Grasping

Grasping an object with a multifingered hand requires a number of forces $\boldsymbol{f}$ applied at contact points P, such that the object is restrained inside the hand. All the contact forces generate a net wrench (generalized force) on the object, given by $\boldsymbol{F} = (\boldsymbol{f}\ \boldsymbol{t})^T$, with $\boldsymbol{f}$ a pure force and $\boldsymbol{t}$ a pure torque [14].

The contact location is described by its relative position $\boldsymbol{r}_p$ and orientation $\boldsymbol{R}_p$ with respect to the object reference frame $\mathcal{O}$, commonly located at the center of mass (COM) of the object (Fig. 2). The force $\boldsymbol{f}_i$ applied by a finger at a contact point is modeled as a wrench $\boldsymbol{F}_i$ exerted at the origin of the contact frame $\mathcal{P}_i$; the transformation between them is given by $\boldsymbol{F}_i = \boldsymbol{B}_i \boldsymbol{f}_i$, with $\boldsymbol{B}_i$ being the *wrench basis* that characterizes the contact model. For simplicity, considering a frictional point contact, the applied wrench is

$$\boldsymbol{F}_i = \begin{bmatrix} 1 & 0 & 0 \\ 0 & 1 & 0 \\ 0 & 0 & 1 \\ 0 & 0 & 0 \\ 0 & 0 & 0 \\ 0 & 0 & 0 \end{bmatrix} \begin{bmatrix} f_{i_x} \\ f_{i_y} \\ f_{i_z} \end{bmatrix} = \boldsymbol{B}_i \boldsymbol{f}_i \tag{1}$$

The forces at the contact must fulfill the positivity restriction, i.e. the fingers can push but cannot pull the object. Besides, it is commonly assumed that Coulomb's friction model holds, stating that slippage is avoided when $f^t \leq \mu f^n$, where f^n is the magnitude of the normal component, f^t is the magnitude of the tangential component, and μ is the friction coefficient. Therefore, the set of allowable contact forces at the contact point is

$$\mathcal{F}_i = \left\{ \boldsymbol{f}_i \in \mathbb{R}^3 \,\middle|\, \sqrt{f_{i_x}^2 + f_{i_y}^2} \leq \mu f_{i_z}\ ,\ f_{i_z} \geq 0 \right\} \tag{2}$$

Geometrically, $\mathcal{F}_i$ represents a *friction cone* with the axis along the surface normal and with a semiangle of $\varphi = \text{atan}(\mu)$. From the computational point of view, it is often advantageous to approximate the nonlinear friction cone with a k-side polyhedral convex cone. Thus, by representing the vector along the j-th edge of the convex cone at the i-th contact with $\boldsymbol{n}_{ij}$, the force at a contact point is given by

$$\boldsymbol{f}_i = \sum_{j=1}^{k} \sigma_{ij} \boldsymbol{n}_{ij}\ ,\ \ \sigma_{ij} \geq 0 \tag{3}$$

The *wrench transformation matrix* $\boldsymbol{W}_p \in \mathbb{R}^{6\times 6}$ that maps the wrenches from the coordinate frame $\mathcal{P}$ to the frame $\mathcal{O}$ is given by the transposed of the adjoint transformation matrix for the homogeneous transformation between both frames,

$$\boldsymbol{W}_p = \boldsymbol{Ad}_{op}^T = \begin{pmatrix} \boldsymbol{R}_p & 0 \\ \hat{\boldsymbol{r}}_p \boldsymbol{R}_p & \boldsymbol{R}_p \end{pmatrix} \tag{4}$$

where $\hat{\boldsymbol{r}}_p$ is the cross product matrix for the vector $\boldsymbol{r}_p = (x_p\ y_p\ z_p)^T$, given by

$$\hat{\boldsymbol{r}}_p = \begin{pmatrix} 0 & -z_p & y_p \\ z_p & 0 & -x_p \\ -y_p & x_p & 0 \end{pmatrix} \tag{5}$$

The wrench exerted by a single contact on the object, expressed in the object coordinate frame, is given by

$$\boldsymbol{F}_{O_i} = \boldsymbol{W}_{p_i} \boldsymbol{B}_i \boldsymbol{f}_i = \boldsymbol{G}_i \boldsymbol{f}_i \tag{6}$$

where $\boldsymbol{G}_i = \boldsymbol{W}_{p_i} \boldsymbol{B}_i$ is called the contact map.

The total wrench $\boldsymbol{F}_O$ on the object is the sum of the contributions from each one of the η contacts, expressed in the same coordinate frame $\mathcal{O}$,

$$\boldsymbol{F}_O = [\boldsymbol{G}_1 \dots \boldsymbol{G}_\eta] \begin{bmatrix} \boldsymbol{f}_1 \\ \vdots \\ \boldsymbol{f}_\eta \end{bmatrix} \tag{7}$$

Let $\boldsymbol{f}_C$ be the contact force vector obtained by stacking all the individual contact forces, i.e. $\boldsymbol{f}_C = (\boldsymbol{f}_1 \dots \boldsymbol{f}_\eta)^T$. The resultant wrench exerted by all the contact forces on the object is given by

$$\boldsymbol{F}_O = \boldsymbol{G} \boldsymbol{f}_C \tag{8}$$

where $\boldsymbol{G}$ is the *grasp map*, given by

$$\boldsymbol{G} = \begin{bmatrix} \boldsymbol{W}_{p_1} \boldsymbol{B}_1 & \cdots & \boldsymbol{W}_{p_\eta} \boldsymbol{B}_\eta \end{bmatrix} \tag{9}$$

Assuming η frictional point contacts, the grasp map is reduced to

$$\boldsymbol{G} = \begin{pmatrix} \boldsymbol{R}_{p_1} & \cdots & \boldsymbol{R}_{p_\eta} \\ \hat{\boldsymbol{r}}_{p_1} \boldsymbol{R}_{p_1} & \cdots & \hat{\boldsymbol{r}}_{p_\eta} \boldsymbol{R}_{p_\eta} \end{pmatrix} \tag{10}$$

III. Dynamic Model

The unconstrained configuration for a bipedal robot with n joints depends on the joint angles $\boldsymbol{q} \in \mathbb{R}^n$ and the position[1] $\boldsymbol{r}_b \in \mathbb{R}^3$ and orientation $\boldsymbol{R}_b \in SO(3)$ of a frame $\mathcal{B}$ attached to a pre-defined base link (e.g. trunk) with respect to the world coordinate system $\mathcal{W}$. Additionally, let $\boldsymbol{\nu} \in \mathbb{R}^3$ and $\boldsymbol{\omega} \in \mathbb{R}^3$ be the translational and angular velocity of the base link represented in $\mathcal{B}$. For notational convenience, we summarize the velocity coordinates in the vector $\boldsymbol{v} = (\boldsymbol{\nu}^T, \boldsymbol{\omega}^T, \dot{\boldsymbol{q}}^T)^T$. Then, the dynamical model can be written in the form

$$\boldsymbol{M}(\boldsymbol{q})\dot{\boldsymbol{v}} + \boldsymbol{C}(\boldsymbol{q},\boldsymbol{v})\boldsymbol{v} + \boldsymbol{p}(\boldsymbol{q},\boldsymbol{R}_b) = \begin{pmatrix}\boldsymbol{0}\\ \boldsymbol{0}\\ \boldsymbol{\tau}\end{pmatrix} + \sum_{k=\{r,l\}} \boldsymbol{J}_k(\boldsymbol{q})^T \boldsymbol{F}_k \ , \tag{11}$$

where $\boldsymbol{M}(\boldsymbol{q})$, $\boldsymbol{C}(\boldsymbol{q},\boldsymbol{v})\boldsymbol{v}$, and $\boldsymbol{p}(\boldsymbol{q},\boldsymbol{R}_b)$ represent the robot's inertia matrix, the vector of centrifugal and Coriolis terms, and the vector of gravity terms, respectively. Additionally, $\boldsymbol{\tau} \in \mathbb{R}^n$ is the vector of actuator torques. The interaction between the robot and its environment is represented in this model via the body wrenches $\boldsymbol{F}_k \in \mathbb{R}^6$ acting at the robot's right ($k = r$) and left foot ($k = l$) via the transposed of the relevant Jacobian matrices $\boldsymbol{J}_k(\boldsymbol{q}) = [\boldsymbol{Ad}_{kb}(\boldsymbol{q}) \quad \boldsymbol{J}^b_k(\boldsymbol{q})]$ onto the system dynamics. Here, $\boldsymbol{Ad}_{kb}(\boldsymbol{q})$ and $\boldsymbol{J}^b_k(\boldsymbol{q})$ are the adjoint matrix related to the homogeneous transformation between the feet and the base link and the body Jacobian for right and left foot [14]. Equation (11) describes the unconstrained dynamics and can be combined with contact constraints for single and double support phases. However, the unconstrained system description has the advantage that the contact forces are explicitly included in the model.

The balancing controller in Section IV aims at controlling the position of the robot's total COM in $\mathcal{W}$, $\boldsymbol{r}_C \in \mathbb{R}^3$, and the orientation $\boldsymbol{R}_b$ of the base link. As shown in [15], the dynamical model gets simplified if the COM velocity is used as a generalized velocity instead of the velocity of the base link. Therefore, we replace $\boldsymbol{v}$ by $\boldsymbol{v}_C = (\dot{\boldsymbol{r}}_C^T, \boldsymbol{\omega}^T, \dot{\boldsymbol{q}}^T)^T$ via

$$\boldsymbol{v} = \begin{pmatrix}\boldsymbol{\nu}\\ \boldsymbol{\omega}\\ \dot{\boldsymbol{q}}\end{pmatrix} = \underbrace{\begin{bmatrix}\boldsymbol{R}_b^T & {}^B\hat{\boldsymbol{r}}_C(\boldsymbol{q}) & -\boldsymbol{J}_{BC}(\boldsymbol{q})\\ \boldsymbol{0} & \boldsymbol{I} & \boldsymbol{0}\\ \boldsymbol{0} & \boldsymbol{0} & \boldsymbol{I}\end{bmatrix}}_{\boldsymbol{A}} \underbrace{\begin{pmatrix}\dot{\boldsymbol{r}}_C\\ \boldsymbol{\omega}\\ \dot{\boldsymbol{q}}\end{pmatrix}}_{\boldsymbol{v}_C} \tag{12}$$

where the matrix $\boldsymbol{J}_{BC}(\boldsymbol{q})$ is given by $\boldsymbol{J}_{BC}(\boldsymbol{q}) = \partial {}^B\boldsymbol{r}_C(\boldsymbol{q})/\partial \boldsymbol{q}$ and ${}^B\boldsymbol{r}_C(\boldsymbol{q})$ denotes the position of the COM as represented in the coordinate system $\mathcal{B}$. In these new coordinates, the dynamic model can be written as

$$\begin{bmatrix} m\boldsymbol{I} & \boldsymbol{0}\\ \boldsymbol{0} & \bar{\boldsymbol{M}}(\boldsymbol{q})\end{bmatrix}\dot{\boldsymbol{v}}_C + \begin{pmatrix}\boldsymbol{0}\\ \bar{\boldsymbol{C}}(\boldsymbol{q},\boldsymbol{v}_C)\boldsymbol{v}_C\end{pmatrix} + \begin{pmatrix} m\boldsymbol{g}\\ \boldsymbol{0}\end{pmatrix} = \begin{pmatrix}\underline{\boldsymbol{0}}\\ \boldsymbol{0}\\ \boldsymbol{\tau}\end{pmatrix} + \sum_{k=\{r,l\}} \bar{\boldsymbol{J}}_k(\boldsymbol{q})^T \boldsymbol{F}_k \ , \tag{13}$$

[1]Unless otherwise mentioned all position vectors are represented with respect to the world frame.

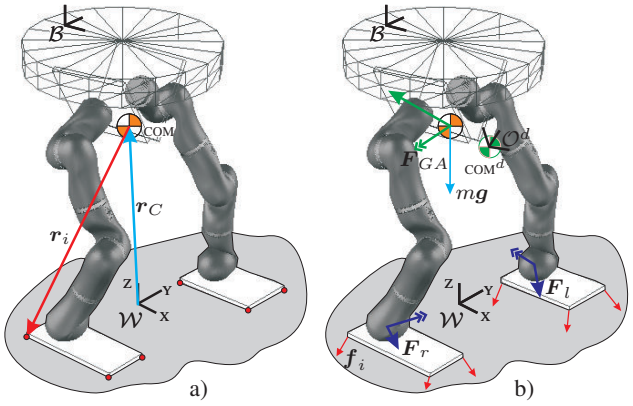

Fig. 3. Contact positions and forces for a biped robot: a) Location of the COM; b) Forces.

wherein the matrix $\bar{\boldsymbol{M}}(\boldsymbol{q})$ and the vector $\bar{\boldsymbol{C}}(\boldsymbol{q},\boldsymbol{v}_C)\boldsymbol{v}_C$ are an inertia matrix and a vector of centrifugal and Coriolis term resulting from the coordinate transformation (12). Additionally, m denotes the total mass and the Jacobian matrices $\bar{\boldsymbol{J}}_k(\boldsymbol{q})$ (with $k = \{r,l\}$) are given by $\bar{\boldsymbol{J}}_k(\boldsymbol{q}) = \boldsymbol{J}_k(\boldsymbol{q})\boldsymbol{A}$ and can be partitioned as

$$\bar{\boldsymbol{J}}_k(\boldsymbol{q}) = \left[\begin{pmatrix}\boldsymbol{R}_k^T\\ \boldsymbol{0}\end{pmatrix} \quad \boldsymbol{Ad}_{kb}\begin{pmatrix}{}^B\hat{\boldsymbol{r}}_C\\ \boldsymbol{I}\end{pmatrix} \quad \underbrace{\boldsymbol{J}^b_k(\boldsymbol{q}) - \boldsymbol{R}_{kb}\boldsymbol{J}_{BC}(\boldsymbol{q})}_{\boldsymbol{J}_{ck}(\boldsymbol{q})}\right]$$

The first three equations in (13) correspond to the dynamics of the COM

$$m\ddot{\boldsymbol{r}}_C + m\boldsymbol{g} = \sum_{k=r,l} \boldsymbol{R}_k \boldsymbol{f}_k \ , \tag{14}$$

which is coupled to the multibody dynamics via the translational components $\boldsymbol{f}_k$ from the contact wrenches $\boldsymbol{F}_k = (\boldsymbol{f}_k, \boldsymbol{t}_k)$. The last n equations in (13) suggest a (quasi-static) mapping of the wrenches $\boldsymbol{F}_k$ to the joint torques $\boldsymbol{\tau}$ via

$$\boldsymbol{\tau} = \sum_{k=r,l} \boldsymbol{J}_{ci}(\boldsymbol{q})^T \boldsymbol{F}_k \tag{15}$$

The particular representation (13) of the equations of motion for a bipedal robot was used as a starting point in [9] for the design of a force based COM balancing controller. In the following section, we extend the controller from [9] by combining the COM balancing control with a posture controller for the base orientation. For this, we utilize the force distribution framework described in Section II.

IV. Balancing Controller

A. Contact force distribution

Consider a biped robot with multiple contacts with the ground (Fig. 3). The system can be analyzed as a series of contact forces applied at the contact points, which generate a net wrench on the robot according to (8). The force component of the net wrench is called the ground reaction force ($\boldsymbol{f}_{GR}$). For balancing, it is more convenient to think of the system as the inverse problem: there is a desired

wrench applied at the COM of the robot, which must be generated through forces at the contact points. The force to be generated is hereafter called ground applied force ($\boldsymbol{f}_{GA}$), defined as $\boldsymbol{f}_{GA} = -\boldsymbol{f}_{GR}$.

Let $\boldsymbol{r}_C$ be the position of the robot COM, described in a world coordinate frame $\mathcal{W}$. The robot only interacts with its environment through forces $\boldsymbol{f}_i$ at $i = 1, \ldots, \eta$ frictional contact points; each contact force is described as $\boldsymbol{f}_i = [f_{i_x}, f_{i_y}, f_{i_z}]^T$, and all the contact forces are stacked in the contact force vector $\boldsymbol{f}_C \in \mathbb{R}^{3\eta}$. The position of the contact points with respect to COM (i.e. in the coordinate frame $\mathcal{O}$) is given by $\boldsymbol{r}_i = [x_i, y_i, z_i]^T$ with $i = 1, ..., \eta$.

Now, the approach for creating a balancing controller is to distribute a desired ground applied force $\boldsymbol{f}_{GA}^d$ to all the contact points, such that they guarantee a net desired wrench $\boldsymbol{F}_{GA}$ on the robot. The relation between $\boldsymbol{F}_{GA}$ and the contact forces $\boldsymbol{f}_C$ is given by (8) ($\boldsymbol{F}_{GA} = \boldsymbol{G}_C \boldsymbol{f}_C$), with $\boldsymbol{G}_C$ the *contact map* (i.e. the grasp map applied to walking robots). For the case of standing on flat ground, the coordinate frame $\mathcal{P}$ at each contact point can be chosen parallel to the world frame $\mathcal{W}$, and in this case $\boldsymbol{G}_C \in \mathbb{R}^{6\times 3\eta}$ is

$$\boldsymbol{G}_C = \begin{pmatrix} I_{3\times 3} & \cdots & I_{3\times 3} \\ \hat{\boldsymbol{r}}_{p_1} & \cdots & \hat{\boldsymbol{r}}_{p_\eta} \end{pmatrix} \tag{16}$$

The corresponding contact forces can be computed by

$$\boldsymbol{f}_C = \boldsymbol{G}_C^{\#} \boldsymbol{F}_{GA} \tag{17}$$

with $\boldsymbol{G}_C^{\#} = \boldsymbol{G}_C^T (\boldsymbol{G}_C \boldsymbol{G}_C^T)^{-1}$ the pseudoinverse of the contact map. This solution minimizes the Euclidean norm of the contact forces under the constraint (8).

The solution to this problem has been considered in the context of grasping, as the minimization of the grasping forces that ensure a stable grasping [16], [17]. These optimization problems include the friction cone restrictions, and guarantee always that the equilibrium (8) is fulfilled. However, for the balancing problem, this is not necessarily true, as the wrench on the object is a control command, which might not be exactly met. Therefore, a new approach is required for this optimization problem.

B. Force distribution using unilateral constraints

The distribution of contact forces according to (17) in general does not guarantee that the constraints (2) are fulfilled. Therefore, we formulate the force distribution problem as a constrained multi-objective optimization problem. The main objective is to achieve the balancing forces from (8), which can be formulated as the minimization of the cost function $J_1(\boldsymbol{f}_C) = ||[\boldsymbol{I}\ \boldsymbol{0}](\boldsymbol{F}_{GA} - \boldsymbol{G}_C \boldsymbol{f}_C)||_2^2$. As a secondary criterion, we select the minimization of the torques from (8), i.e. $J_2(\boldsymbol{f}_C) = ||[\boldsymbol{0}\ \boldsymbol{I}](\boldsymbol{F}_{GA} - \boldsymbol{G}_C \boldsymbol{f}_C)||_2^2$. Additionally, as a third objective, we aim at minimizing the Euclidean norm of the contact forces, similar as in (17), i.e. $J_3(\boldsymbol{f}_C) = \boldsymbol{f}_C^T \boldsymbol{f}_C$. These three objectives are combined in a single quadratic aggregate objective function

$$J(\boldsymbol{f}_C) = \alpha_1 J_1(\boldsymbol{f}_C) + \alpha_2 J_2(\boldsymbol{f}_C) + \alpha_3 J_3(\boldsymbol{f}_C)\ , \tag{18}$$

where $\alpha_1 > 0$, $\alpha_2 > 0$, and $\alpha_3 > 0$ are the weights for the three objectives. By choosing $\alpha_3 << \alpha_2 << \alpha_1$, the first objective is selected as the main priority task and the third objective acts mainly as a regularization of the Hessian for the objective function. The minimization of $J(\boldsymbol{f}_C)$ in combination with the inequality constraints coming from a polyhedral approximation of the friction cone (2) represent a quadratic optimization problem.

In contrast to the solutions in the grasping literature, (8) cannot be considered as an equality constraint in this optimization, since the desired wrench $\boldsymbol{F}_{GA}$ may interfere with the unilateral contact force constraints.

Note that the method assumes that all the predefined contacts are active at every moment, and therefore distributes the desired wrench to all the contact points. A lower limit of the contact force can be preset to some positive value to guarantee that each contact is always active.

C. Balancing and posture controller

The objective of the controller developed in this paper is to bring the ground applied force $\boldsymbol{f}_{GA}$ to a desired value $\boldsymbol{f}_{GA}^d$, which is given by the desired task of balancing while guaranteeing the gravity compensation, i.e.

$$\boldsymbol{f}_{GA}^d = m\boldsymbol{g} + \boldsymbol{f}_r^d \tag{19}$$

with m being the total mass of the robot, $\boldsymbol{g}$ the gravity vector, and $\boldsymbol{f}_r^d$ the desired force for recovering the initial position. Such force can be computed from a PD feedback law, as in [9]

$$\boldsymbol{f}_r^d = -\boldsymbol{K}_P \left(\boldsymbol{r}_C - \boldsymbol{r}_C^d\right) - \boldsymbol{K}_D \left(\dot{\boldsymbol{r}}_C - \dot{\boldsymbol{r}}_C^d\right) \tag{20}$$

where $\boldsymbol{K}_P, \boldsymbol{K}_D > 0$ are the proportional and differential gain matrices, and $\boldsymbol{r}_C^d, \dot{\boldsymbol{r}}_C^d$ are the desired position and velocity of the COM.

To deal with the orientation perturbations, we use a quaternion based representation instead of Euler angles, to avoid potential singularities arising in the computations. Let δ and $\boldsymbol{\epsilon}$ be the scalar and vector part of the quaternion representation of $\boldsymbol{R}_{db} = \boldsymbol{R}_d^T \boldsymbol{R}_b$, with $\boldsymbol{R}_b$ and $\boldsymbol{R}_d$ the current and desired trunk orientation. Then, a suitable potential function for the orientation is given by

$$V_O = 2\boldsymbol{\epsilon}^T \boldsymbol{K}_r \boldsymbol{\epsilon} \tag{21}$$

with $\boldsymbol{K}_r \in \mathbb{R}^{3\times 3}$ a symmetric and positive definite stiffness matrix. As shown in [18], this potential function corresponds to a torsional spring which acts to align $\boldsymbol{R}_b$ to $\boldsymbol{R}_d$, and its torque is given by $\boldsymbol{\tau}_r = -2(\delta \boldsymbol{I} + \hat{\boldsymbol{\epsilon}})\boldsymbol{K}_r \boldsymbol{\epsilon}$, which can be verified by considering the principle of virtual work. Based on this torsional spring, a PD-like orientation controller for the trunk orientation is given by

$$\boldsymbol{\tau}_{GA}^d = \boldsymbol{R}_{wb}(\boldsymbol{\tau}_r - \boldsymbol{D}_r(\boldsymbol{\omega} - \boldsymbol{\omega}^d)) \tag{22}$$

where $\boldsymbol{D}_r \in \mathbb{R}^{3\times 3}$ is a symmetric and positive definite damping matrix.

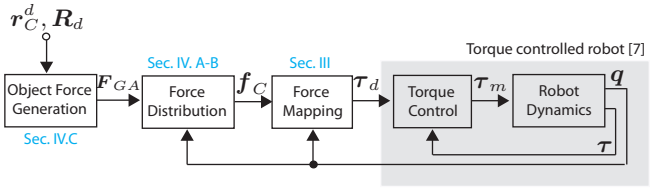

Fig. 4. Overview of the balancing controller.

The forces and torques from (20) and (22) are combined to the net desired wrench $\boldsymbol{F}_{GA}$, which is distributed to the contact forces via the algorithm from Section IV-B. The contact forces are converted into wrenches $\boldsymbol{F}_k$ to be exerted at the right ($k = r$) and left ($k = l$) foot, and are finally projected into joint torques via (15). Figure 4 shows an overview of the complete control scheme. It should be mentioned that, while the presentation in this paper focuses on bipedal foot contact, the control scheme can also be applied to contact situations with more than two contact wrenches $\boldsymbol{F}_k$ (e.g. at the end-effectors) by including the additional contact forces in $\boldsymbol{f}_C$. Notice also that in the derivation of the controller we did not make the assumption that the robot is standing on flat ground. However, a measurement of the robot's COM and trunk orientation with respect to $\mathcal{W}$ are necessary. If the global trunk orientation is available from an onboard inertial measurement unit (IMU), the controller can also be applied to rough uncertain terrain.

D. Comparison with other approaches

The concept of the proposed controller is similar to the one presented in [9]. Both controllers set a desired applied force from the robot to the environment, then distribute that force among predefined contact points, and transform it to the joint torques directly using a Jacobian matrix. The controller in [9] utilizes the ZMP concept for ensuring the positivity of the vertical contact forces, and can be extended to deal with yaw perturbations. On the other hand, the controller proposed in this paper uses a formulation coming from the field of robot grasping, which considers at the same time a desired force and torque that allows the robot to recover the initial position and orientation. The restriction of the ZMP to lie inside the convex hull of the supporting area is implicitly included in our formulation via the the contact force constraints in the optimization.

The balancing controller proposed in [11] compensates the linear and angular components of the spatial momentum. The approach computes the individual ground reaction force and center of pressure at each support foot, which allows it to deal with different ground geometry. The desired forces at the feet are later used to determine the joint accelerations and torques, using inverse dynamics, and the overall torque input is controlled using feedback linearization. In our approach, we compute a single ground reaction force which is later distributed as forces in predefined contact points via a constrained optimization. The optimization problem tries to achieve the force and torque required to recover the initial position and orientation, and minimizes the Euclidean norm of the contact forces, while considering the restrictions coming from the friction with the surface. The approach does not require the use of inverse kinematics or dynamics. Our controller also focuses on keeping a desired orientation at the hip, rather than regulating the total angular momentum of the robot; this consideration can be advantageous in applications such as biped vehicles [19].

V. Experiments

The proposed balancing controller was tested in simulations using OpenHRP3 [20], and in experiments with the DLR Biped shown in Fig. 1 [6]. The DLR Biped has six degrees of freedom per leg, a 6-DOF force-torque sensor (FTS) in each foot, position and torque sensors in each joint, and an inertial measurement unit (IMU). For the approach from this paper, the FTS at the feet are not used. The resulting joint torques from (15) are commanded to an underlying joint torque controller [7].

A. Implementation details

The origin of the world coordinate frame $\mathcal{W}$ was chosen to be in the middle point between the two feet. The trunk orientation and angular velocity are measured via the IMU. The used IMU gives reliable information on the roll and pitch angles, but it shows considerable drift in the yaw rotation. Therefore, we approximate the yaw angle between the world frame and the trunk by comparing the trunk orientation to the baseline between the right and the left foot.

The proportional gain matrix $\boldsymbol{K}_p$ for the COM balancing controller was chosen as a diagonal matrix with stiffness values of $k_h = 900N/m$ in the horizontal ($x-$ and $y-$) directions, and $k_v = 3000N/m$ in the vertical ($z-$) direction. The damping gain matrix $\boldsymbol{K}_D$ was chosen as a diagonal matrix with the elements set to $d_h = \sqrt{(}mk_h)2 \cdot 0.8$ for the horizontal components and $d_v = \sqrt{(}mk_v)2 \cdot 0.2$ for the vertical component. The rotational stiffness and damping matrices were set to $\boldsymbol{K}_r = 100\boldsymbol{I}[Nm/rad]$ and $\boldsymbol{D}_r = 50\boldsymbol{I}[Nms/rad]$. The same controller gains were used in the simulations and in the experiments.

The constrained optimization problem from Sec. IV-B was solved using the open source software qpOASES [21]. With $\eta = 8$ unilateral contact points, the computation time for the optimization of $3\eta = 28$ components in $\boldsymbol{f}_C$ took less than $200\mu s$ on the onboard $2.8GHz$ mobile CPU running under the real-time operating system VxWorks.

B. Simulation results

Both the balancing and the COM tracking behavior of the controller under external disturbances were evaluated in simulations. In the first simulation, the desired velocity for the COM in (20) is set to $\dot{\boldsymbol{r}}_C^d = 0$ and a lateral force of $70N$ was applied during $50ms$ at the hip (Fig. 5). Notice that this force applies also a considerable torque onto the base link, since it is not exerted at the COM. Figure 6 shows the COM error resulting from this simulation. The corresponding object force is presented in Fig. 7 and shows that a considerable torque around the $x-$ axis is required

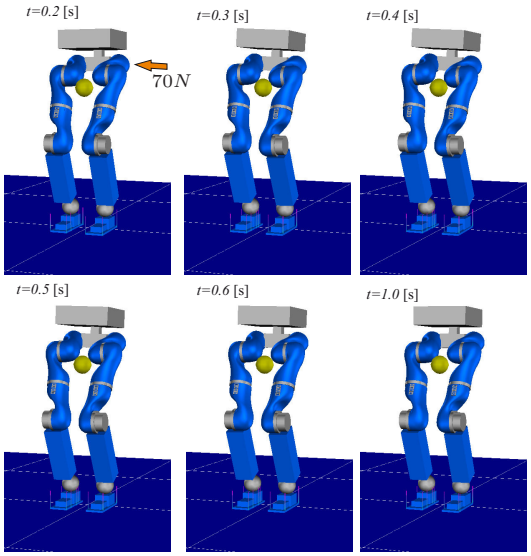

Fig. 5. Balancing experiment in OpenHRP.

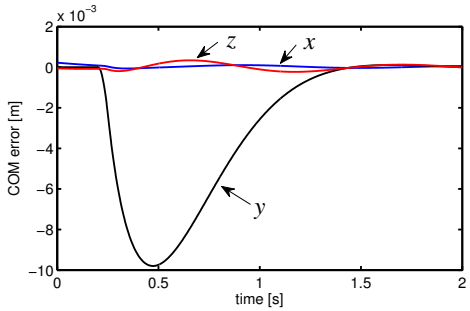

Fig. 6. COM error for the simulated lateral force disturbance. The blue, black, and red line represent the $x-$, $y-$, and $z-$coordinate.

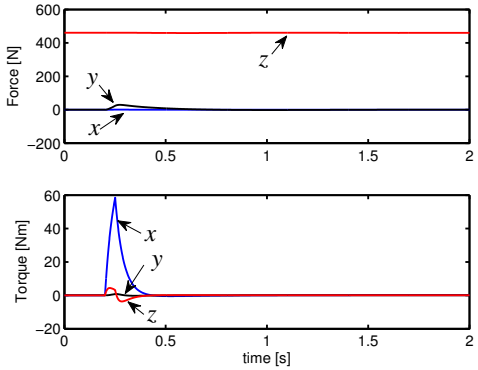

Fig. 7. Object force and torque for the simulated lateral force disturbance. The blue, black, and red line represent the $x-$, $y-$, and $z-$coordinate.

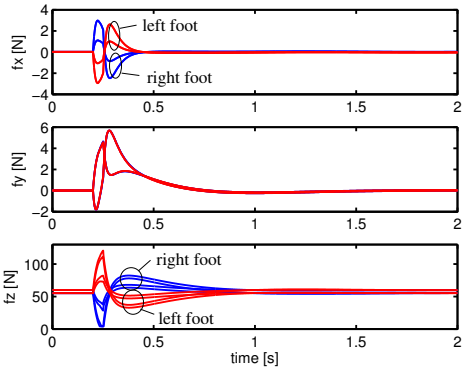

Fig. 8. Contact force components for the simulated lateral force disturbance. The forces at the contact points on the right foot are shown in blue and the forces at the contact points on the left foot are shown in red.

to counterbalance the disturbance. The components of the contact forces are displayed in Fig. 8. At the time $t \approx 0.25s$ the vertical forces of the right foot (in blue) reach their lower limit of $4N$ set in the optimization algorithm from Sec. IV-B. The values of the weights for the multi-objective optimization are chosen as $\alpha_1 = 1$, $\alpha_2 = 10^{-3}$ and $\alpha_3 = 10^{-6}$.

As a second simulation, a COM tracking task is presented. Figure 9 shows the horizontal components of the desired and actual COM. At the time $t = 5s$, the same disturbance as in the previous simulation is exerted on the robot, which leads to a small deviation of the actual COM motion. In Fig. 10 the corresponding contact force components are shown. The most interesting part is around the time of the disturbance, for which a detailed plot is given in Fig. 11. Note that the vertical contact forces are kept positive by the constraint optimization algorithm.

C. Experimental evaluation

Finally, we present two experiments with the DLR Biped by which the proposed balancing algorithm was evaluated. The first experiment presents an impulsive disturbance. A pendulum provided an impact of about $5.8J$ on the robot. The length of the pendulum was about $7.3m$ with an end-point mass of $5kg$. Figure 12 shows the evolution in time of the balance recovery when the pendulum collides with the robot.

Figure 13 shows the COM error for this case. Note that the COM error stays relatively small, since the impulsive disturbance acts only for a rather small time. The effects of the disturbance on the object force and the contact force components for the right and left foot are shown in Fig. 14 and Fig. 15, respectively. Even if the COM error stays small, the balancing forces at the contact points vary considerably for counteracting the disturbance.

As a last experiment, physical interaction with a human is shown in Fig. 16, where the trunk of the robot is pushed creating different perturbations in position and orientation. The corresponding COM error for pushes in $x-$ and $y-$ direction are shown in Fig. 17. The corresponding contact forces in Fig. 18 show the result of the balancing controller. Here, the non-negativity constraints on the vertical contact force components act over a longer duration, due to the human interaction representing a low frequency disturbance.

VI. Summary

This paper presents an optimization based balancing algorithm for bipedal robots. It allows to distribute a net wrench

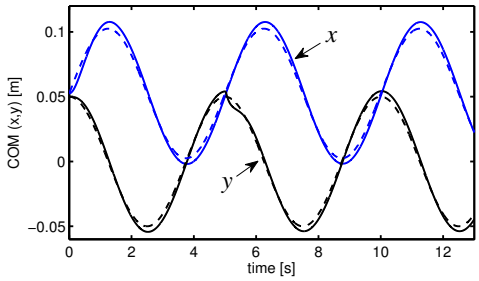

Fig. 9. Horizontal com coordinates for the tracking simulation with external disturbance. The dashed lines show the desired COM trajectory and the solid lines the actual COM trajectory ($x-$coordinate in blue and $y-$coordinate in black).

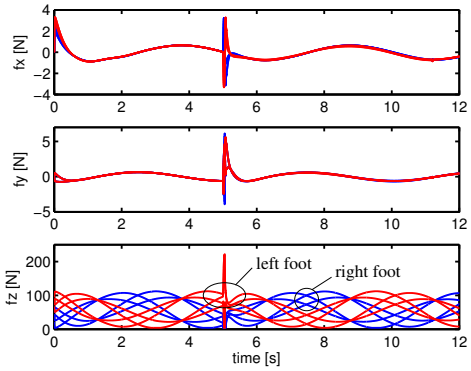

Fig. 10. Contact force components for the tracking simulation.

required to recover a desired center of mass position and posture onto a predefined set of contact points.

The approach was verified in simulation and in experiments with a torque controlled robot. The balancing controller, including the approach for distributing the contact force, is general enough to be applied to a biped robot in different contact situations, such as single or double support phases. It can also be applied to multi-legged robots.

The current approach is using a finite set of contact points. However, an extension to more general contact forces seems possible and is part of our future work.

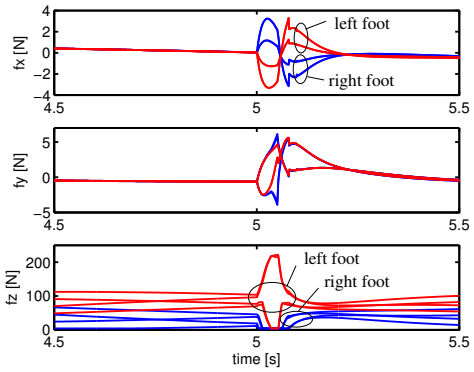

Fig. 11. Detailed view for the contact force components for the simulated lateral force disturbance.

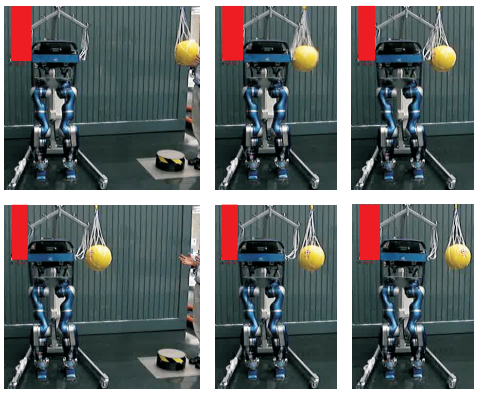

Fig. 12. Results of the balancing experiment. Filled rectangles are overimposed as visual clues to perceive the displacement of the robot.

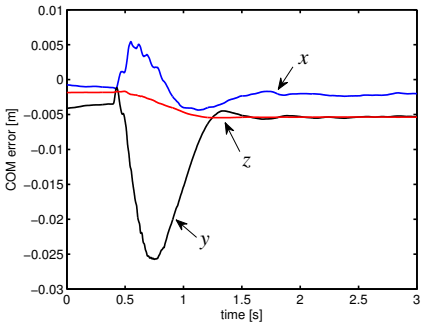

Fig. 13. COM error for the experiment with impulsive disturbance. The blue, black, and red line represent the $x-$, $y-$, and $z-$coordinate.

REFERENCES

[1] S. Setiawan, S. Hyon, J. Yamaguchi, and A. Takanishi, "Physical interaction between human and a bipedal humanoid robot - realization of human-follow walking," in *IEEE Int. Conf. on Robotics and Automation*, 1999, pp. 361–367.

[2] K. Hirai, M. Hirose, Y. Haikawa, and T. Takenaka, "The development of the Honda humanoid robot," in *IEEE Int. Conf. on Robotics and Automation*, 1998.

[3] T. Sugihara and Y. Nakamura, "Whole-body cooperative balancing of humanoid robot using cog jacobian," in *IEEE Int. Conf. on Robotics and Automation*, 1999, pp. 361–367.

[4] G. Cheng, S.-H. Hyon, J. Morimoto, A. Ude, J. G. Hale, G. Colvin, W. Scroggin, and S. C. Jacobsen, "CB: A humanoid research platform for exploring neuroscience," *Advanced Robotics*, vol. 21, no. 10, 2007.

[5] J. Pratt and B. Krupp, "Design of a bipedal walking robot," in *Proceedings of the 2008 SPIE*, vol. 6962, 2008.

[6] C. Ott, C. Baumgärtner, J. Mayr, M. Fuchs, R. Burger, D. Lee, O. Eiberger, A. Albu-Schäffer, M. Grebenstein, and G. Hirzinger, "Development of a biped robot with torque controlled joints," in *IEEE-RAS Int. Conf. on Humanoid Robots*, 2010, pp. 167–173.

[7] A. Albu-Schäffer, Ch. Ott, and G. Hirzinger, "A unified passivity-based control framework for position, torque and impedance control of flexible joint robots," *Int. J. Robotics Research*, vol. 26, no. 1, pp. 23–39, January 2007.

[8] C. Ott, A. Albu-Schäffer, A. Kugi, and G. Hirzinger, "On the passivity based impedance control of flexible joint robots," *IEEE Trans. Robotics*, vol. 24, no. 2, pp. 416–429, 2008.

[9] S.-H. Hyon, J. G. Hale, and G. Cheng, "Full-body compliant human-humanoid interaction: Balancing in the presence of unknown external forces," *IEEE Trans. Robotics*, vol. 23, no. 5, 2007.

[10] S.-H. Hyon, "Compliant terrain adaptation for biped humanoids without measuring ground surface and contact forces," *IEEE Trans. Robotics*, vol. 25, no. 1, 2009.

[11] S.-H. Lee and A. Goswami, "Ground reaction force control at each foot: A momentum-based humanoid balance controller for non-level

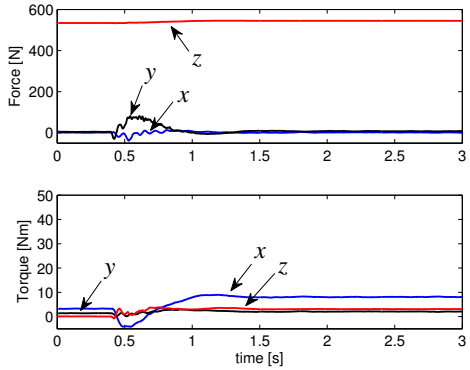

Fig. 14. Object force and torque for the experiment with impulsive disturbance. The blue, black, and red line represent the $x-$, $y-$, and $z-$coordinate.

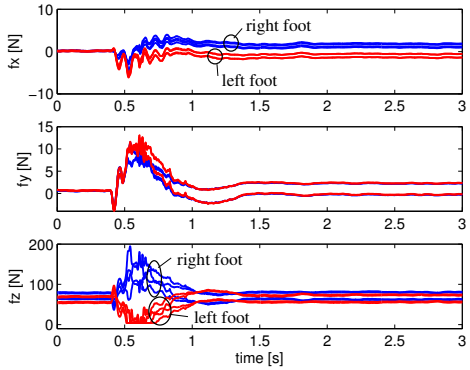

Fig. 15. Contact force components for the impact experiment.

and non-stationary ground," in *IEEE/RSJ Int. Conf. on Intelligent Robots and Systems*, 2010, pp. 3157–3162.

[12] B. Stephens and C. G. Atkeson, "Dynamic balance force control for compliant humanoid robots," in *IEEE/RSJ Int. Conf. on Intelligent Robots and Systems*, 2010, pp. 1248–1255.

[13] L. Sentis, J. park, and O. Khatib, "Compliant control of multicontact and center-of-mass behaviors in humanoid robots," *IEEE Trans. Robotics*, vol. 26, no. 3, pp. 483–501, 2010.

[14] R. Murray, Z. Li, and S. Sastry, *A Mathematical Introduction to Robotic Manipulation*. Boca Ratón, Florida: CRC Press, 1994.

[15] P.-B. Wieber, *Fast Motions in Biomechanics and Robotics*, ser. Lecture Notes in Control and Information Sciences. Springer Berlin / Heidelberg, 2006, vol. 340, ch. Holonomy and Nonholonomy in the Dynamics of Articulated Motion, pp. 411–425.

[16] L. Han, J. Trinkle, and Z. Li, "Grasp analysis as linear matrix inequality problems," *IEEE Trans. Robotics and Automation*, vol. 16, no. 6, pp. 663–674, 2000.

[17] J. Saut, C. Remond, V. Perdereau, and M. Drouin, "Online computation of grasping force in multi-fingered hands," in *IEEE/RSJ Int. Conf. on Intelligent Robots and Systems*, 2005, pp. 1223–1228.

[18] F. Caccavale, C. Natale, B. Siciliano, and L. Villani, "Six-dof impedance control based on angle/axis representations," *IEEE Trans. Robotics and Automation*, vol. 15, no. 2, pp. 289–299, 1999.

[19] K. Hashimoto, H. O. Lim, and A. Takanishi, "Disturbance compensation control for a biped vehicle," *Advanced Robotics*, vol. 25, no. 3, 2011.

[20] F. Kanehiro, K. Fujiwara, S. Kajita, K. Yokoi, K. Kaneko, H. Hirukawa, Y. Nakamura, and K. Yamane, "Open architecture humanoid robotics platform," in *IEEE Int. Conf. on Robotics and Automation*, 2002, pp. 24–30.

[21] H. Ferreau, H. Bock, and M. Diehl, "An online active set strategy to overcome the limitations of explicit MPC," *Int. J. Robust and Nonlinear Control*, vol. 18, no. 8, 2008.

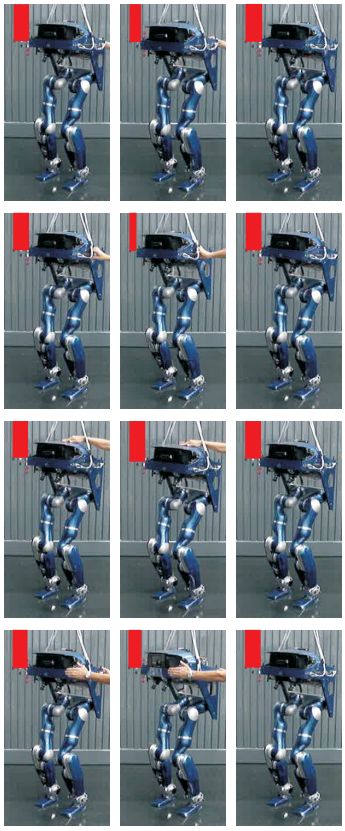

Fig. 16. Compensatory motions for different perturbations applied to the robot, from top to bottom: in X, in Y, in Z and in yaw. Filled rectangles are overimposed as visual clues to perceive the displacement of the robot.

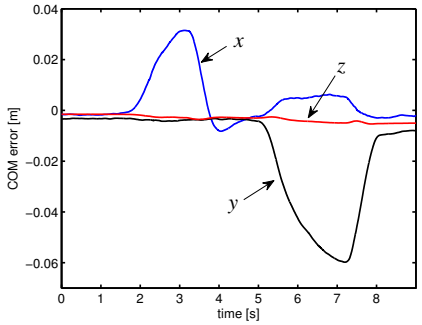

Fig. 17. COM error for the physical human interaction experiment. The blue, black, and red line represent the $x-$, $y-$, and $z-$coordinate.

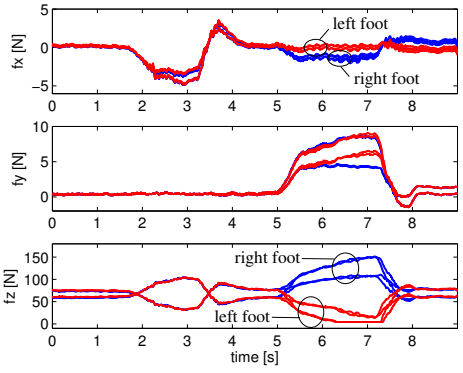

Fig. 18. Contact force components for human interaction experiment.